Magnetocrystalline anisotropy of monatomic steps in Fe/Ag(001) nanopatterned films

F. Bisio,[1,2] A. Toma,[3] R. Moroni,[1,2,*] R. Pasero,[3] F. Buatier de Mongeot,[2,3] C. Boragno,[2,3] M. Canepa,[2,3] U. Valbusa,[3] and L. Mattera[2,3]

[1]*CNR-INFM, Unità di Genova, via Dodecaneso 33, I-16146 Genova, Italy*

[2]*CNISM, Sede Consorziata di Genova, via Dodecaneso 33, I-16146 Genova, Italy*

[3]*Dipartimento di Fisica, Università di Genova, via Dodecaneso 33, I-16146 Genova, Italy*

(Received 14 November 2006; published 12 February 2007)

We have experimentally determined the magnitude of the in-plane magnetocrystalline anisotropy of monatomic Fe steps on the surface of nanopatterned Fe/Ag(001) films. The films have been nanopatterned by the ion-sculpting technique, in which grazing-incidence ion sputtering is exploited to induce the formation of nanometer-scale surface ripples oriented along the ion-beam direction. We quantitatively assessed the ripple morphology in order to determine the density of Fe monatomic steps parallel to the ripple ridges. By correlating the morphology with the measured uniaxial magnetic anisotropy, we obtained the strength of the magnetocrystalline anisotropy of Fe monatomic steps $\kappa_u^{mc}=(6.5\pm1.5)\times10^{-10}$ erg/cm.

DOI: 10.1103/PhysRevB.75.054407 PACS number(s): 75.30.Gw, 75.75.+a, 81.16.Rf

I. INTRODUCTION

The magnetocrystalline anisotropy energy of atoms located at low-coordinated crystal sites strongly differs from the one of fully coordinated bulk atoms.[1–10] In the case of low-dimensional, nanometer-sized magnetic systems, for which the relative abundance of low-coordinated interfacial atoms can be made arbitrarily large, the overall anisotropy can be completely determined by the atoms located at the spatial boundary of the system itself.

Magnetocrystalline anisotropy is a subtle quantity involving energy differences much lower than the total electronic energy of the system. In magnetic nanostructures, symmetry-breaking effects due to the presence of spatial boundaries further complicate its evaluation. Thus, theoretically modeling the magnetic anisotropy energy of low-dimensional systems remains a challenging task.[3,4] To this end, the availability of reliable experimental data greatly contributes to the possibility of delving deeper into the subject, allowing a meaningful comparison with existing theoretical models.

Recently, the anisotropy properties of ensembles of magnetic atoms deposited onto various nonmagnetic surfaces have attracted considerable interest. Experiments have addressed monatomic-height wires, stripes, and islands.[5,7–9] A natural extension of the above-mentioned investigations is to address the magnetic anisotropy of low-coordinated atoms located at the spatial boundary of thicker and more extended magnetic systems. Besides the well-known studies of the surface-type anisotropy in ultrathin films,[1,2] the anisotropy properties of monatomic steps at the surface of ultrathin magnetic films also attracted a great deal of interest in the past.[11–15] More recently, such an interest has been renewed, thanks to the possibility of addressing the step-induced anisotropy with higher precision in aptly fabricated magnetic nanostructures.[10] In detail, nanostructures fabricated by the ion-sculpting technique appear as promising systems for this type of study.[6,10] In the ion-sculpting technique, the interaction of a grazing-incidence defocused ion beam with an epitaxial film induces the self-organization of nanometer-scale surface ripples oriented along the projection of the ion-beam direction on the surface (see Fig. 1).[16,17] At the atomic scale, the ripple formation leads to the arrangement of monatomic steps preferentially oriented along the ripple ridges, giving rise to a clearly observable uniaxial magnetic anisotropy.[6] Under appropriate conditions, for this type of system, the magnetocrystalline anisotropy due to atomic steps can be selectively measured.[6,10]

In this article, we report an experimental study of the in-plane uniaxial magnetic anisotropy induced by monatomic steps aligned along the [100] direction at the surface of ultrathin Fe/Ag(001) films, nanostructured by the ion sculpting technique. The Fe/Ag(001) system was chosen as a prototypical example of bcc-Fe-based low-dimensional system, whose morphological and magnetic properties have been thoroughly addressed.[2,13,18–22] In this work, we exploit the correlation between the nanosized ripple morphology and the magnetic anisotropy to determine the magnitude of the magnetocrystalline anisotropy due to monatomic steps (κ_u^{mc}) at the surface of Fe/Ag(001) films. Our estimate of κ_u^{mc} is smaller by 2 orders of magnitude with respect to the previously accepted value, measured from vicinal films.[13] The physical origin of such a discrepancy is discussed on the basis of recent work,[14] which highlights possible limits of the vicinal-surface approach.

II. EXPERIMENT

The experiments have been performed under ultrahigh vacuum conditions (base pressure lower than 1×10^{-10} mbar). Magnetic properties have been studied by the magneto-optical Kerr effect (MOKE) in longitudinal configuration, whereas morphological properties have been addressed by low-energy electron diffraction with spot profile analysis (SPA-LEED) (1000 Å coherence length) and Auger electron spectroscopy (AES).

The Ag(001) substrate was prepared by cycles of sputtering with 1 keV Ar^+ ions and annealing at 800 K until a sharp LEED pattern was observed and all contaminants were found below the AES detection sensitivity. Iron films of variable thickness have been deposited at normal incidence in order

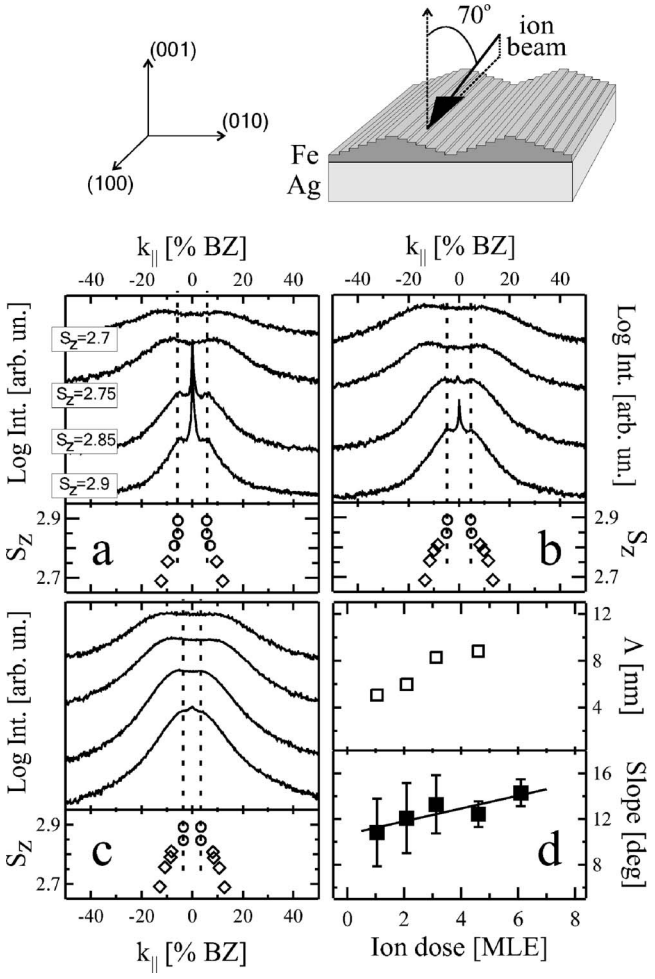

FIG. 1. (Top part) Experimental geometry and schematic of the ripple structure. Crystallographic orientations refer to the bcc unit cell of Fe. (Bottom part) Panels a–c: SPA-LEED *k*-space cuts measured along the [010] direction for an ion dose of (a) 1 MLE, (b) 2 MLE, and (c) 3 MLE. Open circles and diamonds at the bottom of panels a, b, and c represent the *k*-space position of the lateral correlation satellites and the facet satellites, respectively. Panel d: ion-dose dependence of the ripple wavelength Λ (open squares) and the facet slope α (full squares). The solid line is a linear fit to the ion-dose dependence of the facet slope.

to prevent any growth-induced magnetic anisotropy.[23] Fe grows on Ag epitaxially,[19] with crystallographic orientations $[100]_{Fe}\|[110]_{Ag}$ and $[001]_{Fe}\|[001]_{Ag}$ (we will henceforth refer to the crystallographic orientation of the Fe bcc unit cell). The film thickness has been calibrated by the observation in the curves of longitudinal MOKE versus deposition time of the spin reorientation transition.[24,25] The thickness uncertainty is of the order of ±5%. In this article, we will focus on 24-ML-thick Fe films, deposited via a two-step procedure. The first 10 ML are deposited with the substrate held at 300 K; the temperature is then sharply raised to 510 K and maintained constant during the ongoing deposition until the desired thickness is achieved. The initial growth temperature of 300 K has been explicitly chosen to make contact with the experimental data of Ref. 24 and to induce a mild segregation of Ag, in order to take advantage of its surfactant properties in the 510 K growth step.[18,22] LEED measurements show that extremely flat Fe films, free of any detectable long-range lateral periodicity, are grown by means of this procedure.

The Fe films have been sculpted by irradiation with 1 keV Ar^+ ions at an incidence angle of 70° from the surface normal and along the [100] direction. A sketch of the experimental geometry is depicted in the top part of Fig. 1. The ion sputtering has been performed with the sample held at 350 K and with an ion current impinging on the sample of about 1.1 μA. MOKE and SPA-LEED measurements reported here have been performed *in situ* at 350 K and room temperature, respectively.

III. RESULTS

A. Morphology

The film morphology as a function of the ion dose has been characterized via a combination of SPA-LEED and AES data. The LEED pattern of as-deposited films did not show any detectable long-range periodicity due to hillock formation,[20] and exhibited a very sharp and intense Bragg peak in the in-phase conditions with very low background, indicative of a smooth surface with very low uncorrelated roughness. AES spectra of the as-deposited films exhibit the expected Fe peaks and an intense Ag peak. The evolution of such Ag peak during sputter depth profiling allows us to ascribe it to Ag atoms segregated at the surface and partly dissolved in the interior of the film.[20,22] Quantitative analysis of the spectra allows us to determine that approximately 0.75 ML of Ag is segregated at the surface of the film, whereas the Ag concentration within the film is found to be below 5%, in agreement with Ref. 20. The segregated Ag was completely removed after irradiation with an ion dose (Φ) larger than 2 MLE (1 MLE$=1.2\times10^{15}$ ions/cm^2).

In Fig. 1, three representative sets of one-dimensional SPA-LEED *k*-space profiles of the (00) Bragg peak along the [010] direction are plotted at increasing ion dose (panels a–c). Constructive (in-phase) and destructive (out-of-phase) interferences from the exposed terraces are defined, respectively, by integer and half-integer values of the vertical scattering phase $S_z=k_z d/2\pi$, with k_z as the vertical momentum transfer and $d=0.143$ nm as the Fe montomic step height.[26] In the following, the parallel scattering vector $k_\|$ will be expressed in percent units of the first Brillouin zone (% BZ) along the [010] direction.

Figure 1(a) shows a diffraction profile of the (00) spot after patterning the initially flat Fe/Ag(001) film with 1 MLE of Ar^+ ions, following the procedure reported in Sec. II. A ripple corrugation elongated in the [100] direction is formed, as revealed by the analysis of the diffraction profile, which shows the presence of two pairs of satellites. The inner ones, whose position q_0 is independent of S_z, provide the lateral periodicity of the ripple $\Lambda=2\pi/q_0$, which reads 5 nm for this dose, while the outer ones are due to the presence of regular step arrays (and facets) along the [100] direction. When moving toward an out-of-phase diffraction condition, the outer satellites dominate the diffraction pattern and their splitting increases linearly with S_z, providing a measure of

the average facet slope (α). The open circles and diamonds at the bottom of panels a, b, and c represent, respectively, the k-space position of the satellite peaks due to the lateral correlation and the facets, while the vertical dashed lines are drawn at $k_{\parallel}=q_0$. We notice that no satellite peaks were observed for azimuthal cuts along [100], clearly indicating that elongated ripples were formed. Increasing the ion dose to 2 MLE [Fig. 1(b)], we observe that the relative intensity of the Bragg peak has decreased with respect to the case of Fig. 1(a), a clear signature of the increase of the surface roughness of the Fe film induced by the ion-sculpting process. Despite the increase of diffuse scattering, we can still clearly observe in the azimuthal cuts the lateral correlation satellites, giving a value of ripple wavelength of 6 nm, and the facet-induced peaks. After sputtering with an ion dose of 3 MLE [Fig. 1(c)], the Bragg peak has almost completely decayed even for nearly in-phase conditions at $S_z=2.9$, confirming the observed increase of surface roughness. Even in the presence of increased diffuse scattering, we can still extract from the data a ripple wavelength of 8.3 nm, and clearly observe well-defined facet peaks. At even larger ion dose (not reported in the graph), we detect a further increase in the uncorrelated background, which gradually prevents a clear identification in the diffraction pattern of the satellites originated by the lateral ripple correlation. Thus, at 4.5 MLE, a ripple wavelength of 8.8 nm is still observable, whereas at 6 MLE, the background prevents a clear assessment of the wavelength. Instead, facet peaks remain still clearly discernible up to an ion dose of 6 MLE. The ion-dose dependences of both the ripple wavelength and the facet slope are reported in Fig. 1(d) as open and solid squares, respectively. According to the data reported in Fig. 1(d), both facet slope and ripple wavelength show the tendency to increase with increasing ion dose, similar to that observed in ion sculpting of single crystals.[6,16,17] The wavelength Λ for the explored ion doses lies in the 5–10 nm range, whereas the ripple slope slowly increases from approximately 11° at 1 MLE to 14° at 6 MLE.

Data show a substantial analogy between the effects of ion sculpting of thin films and of the single-crystal surfaces.[6,16,17] Thus, we can infer that for the Fe/Ag(001) system in the very low-dose regime (approximately below 2–3 MLE), a transition from the random stacking of adatom and vacancy clusters, produced after the single ion impact events, to the well-developed ripples takes place. The analogy is also expected to hold in the intermediate regime between 2–3 and 6–7 MLE, where the ripple morphology can be represented in a simplified one dimensional model as a triangular waveform unequivocally identified by its wavelength and slope. However, in the high-dose regime, above 6–7 MLE, both the accumulation of uncorrelated roughness at the surface and the perturbing action of the buried Fe-Ag interface in determining the system morphology cannot be neglected [for the present experiment, this effect becomes dominant around 9–10 MLE (see Fig. 3)]. We therefore expect that the simplified ripple model sketched in Fig. 1, in which chemically pure Fe ripples stand on top of the Ag substrate, will cease to hold as we approach this regime.

B. Magnetism

In Fig. 2, we report a set of longitudinal MOKE hysteresis loops measured with the external field $\mathbf{H}\|[010]$ (perpendicular to the ripple direction) as a function of the ion dose. The hysteresis loops, which are square for the as-deposited film, split in two separate semiloops for increasing ion dose, and then gradually assume the typical uniaxial hard-axis shape. Hysteresis loops measured with external field parallel to the ripple direction (not shown) remain square throughout the whole investigated ion-dose range. Qualitatively, the evolution of the hysteresis loops as a function of the ion dose indicates that the ripple formation induces the onset of an in-plane uniaxial anisotropy, favoring the alignment of the spontaneous magnetization parallel to the ripple direction.[10,27]

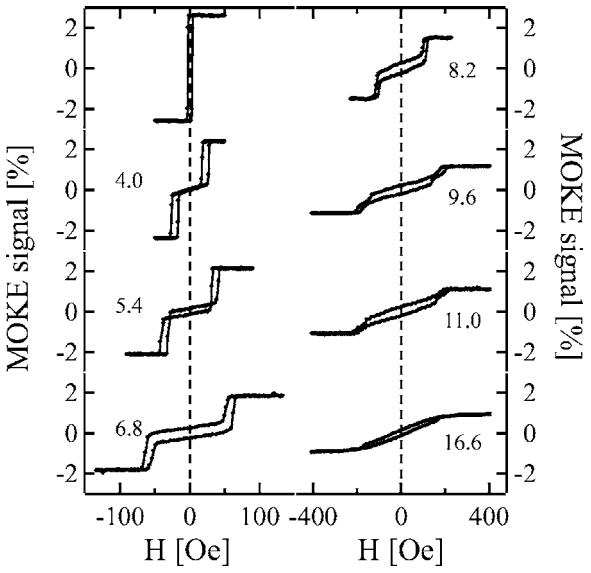

FIG. 2. Hysteresis loops of ion-sculpted Fe/Ag(001) films measured with external field parallel to the [010] direction as a function of the ion dose Φ (in MLE). MOKE signals (vertical scales) are expressed as percentage variation from the steady (non-magneto-optical) signal. Notice the different horizontal scales for the left and right column data.

In order to extract quantitative information from the hysteresis loops, we assume the functional form of the free-energy density of the in-plane magnetized film to be

$$E = \frac{K_c}{4}\sin^2(2\varphi) + K_u \sin^2(\varphi) - \mathbf{M}\cdot\mathbf{H}, \qquad (1)$$

where K_c and K_u are the biaxial and uniaxial anisotropy constants, respectively, and φ is the angle between the magnetization $\mathbf{M}$ and the uniaxial easy axis, and deduce K_c, K_u, and the MOKE saturation intensity I_{sat} according to well-established procedures.[28,23] In Fig. 3, the ion-dose dependences of the MOKE saturation intensity I_{sat} (top panel) and the uniaxial anisotropy constant K_u (bottom panel) thus extracted are reported. The ion-dose dependence of the biaxial anisotropy constant K_c is not reported here, having been thoroughly discussed elsewhere.[27]

As shown in Fig. 3, the MOKE saturation signal stays nearly constant up to approximately 2 MLE, and linearly decreases with increasing ion doses between 2 MLE and approximately 10 MLE. Above 10 MLE, the rate of decrease of

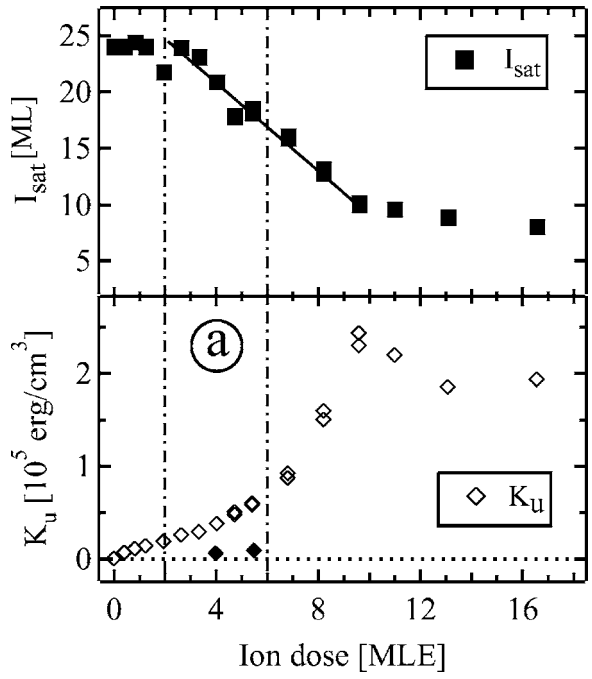

FIG. 3. (Top panel) MOKE saturation value I_{sat} as a function of the ion dose. I_{sat} is expressed in terms of the average Fe film thickness due to the proportionality between the two (see text for details). The solid line is a linear fit to the ion-dose dependence of I_{sat} in the 2–10 MLE ion-dose range. (Bottom panel) Uniaxial anisotropy constant K_u as a function of the ion dose (open diamonds). Full diamonds represent the upper limit of magnetostatic and/or magnetoelastic anisotropy at 4 and 5.5 MLE (see text for details). The vertical dash-dotted lines mark the lower and upper limits of the ion-dose interval employed for the quantitative analysis of the step-induced uniaxial anisotropy. Such an ion-dose range is referred to as region (a).

I_{sat} suddenly drops, and the MOKE saturation signal slowly diminishes up to the largest investigated dose of 17 MLE. Correspondingly, the uniaxial anisotropy constant exhibits a monotonous increase up to approximately 10 MLE, and then slightly decreases. The decrease of I_{sat} with increasing ion dose can be viewed as a fingerprint of the regular decrease of the film thickness due to the material removal associated with the sputtering procedure, given the well-established proportionality of the MOKE signal at saturation to the average ferromagnetic film thickness in the ultrathin regime.[29] The ion-dose dependence of K_u can be accounted for by correlating it with the ongoing morphological evolution of the film, as discussed in the next section.

IV. DISCUSSION

In this section, we will discuss the correlation between morphology and uniaxial magnetic anisotropy that allows us to derive the magnitude of the step-induced magnetocrystalline anisotropy for the Fe/Ag(001) system.

A. Morphology

In the ion-dose interval below 2 MLE, it was already suggested by the analysis of LEED data that the surface evolves from a flat morphology to the one characterized by well-defined ripples with regularly faceted sidewalls. Correspondingly, AES data show that the Ag atoms initially segregated at the film surface are removed by the etching action of the ion beam. The value of the MOKE saturation intensity I_{sat} in this ion-dose interval stays nearly constant. The constancy of I_{sat} is apparently surprising because of the expected decrease of film thickness due to the removal of Fe atoms. Such behavior can be accounted for by taking into consideration the fact that the sputtering yield of Fe atoms (Y_{Fe}), which is ultimately responsible for the ion-dose dependence of I_{sat}, is expected to be lower at the lowest doses due to both the roughness dependence of Y_{Fe} (Refs. 30 and 31) and the initial removal of the segregated Ag atoms by the ion beam.[22]

In the range between approximately 2 MLE and 10 MLE, we witness an almost perfectly linear decrease of I_{sat} with increasing dose. Within this ion-dose window, the morphological evolution of the film is mainly characterized by the slow increase of the ripple sidewall slope and the gradual buildup of uncorrelated roughness. The main effect of sputtering in this ion-dose interval is therefore the removal of Fe atoms from the film, which leads to the extremely regular decrease of I_{sat} experimentally observed. The increase of uncorrelated roughness is due to the accumulation of sputtering-induced defects, such as vacancies, step adatoms, or kinks, which do not relax at 350 K due to insufficient mobility. A linear fit of $I_{sat}(\Phi)$ in this ion-dose interval (solid line in Fig. 3) gives a sputtering yield for Fe $Y_{Fe}=2.0\pm0.1$.

For ion doses higher than 10 MLE, the Fe sputtering yield, as deduced from the $I_{sat}(\Phi)$ dependence, drops abruptly to approximately $Y_{Fe}=0.3\pm0.05$. The average Fe film thickness at 10 MLE, deduced from I_{sat}, reads approximately 9 ML. Extrapolation of the ripple wavelength and sidewall slope to 10 MLE gives a mean distance of the ripple grooves from the Ag substrate at this ion dose of approximately 5 ML of Fe. The small distance between the ripple grooves and the substrate suggests that the abrupt decrease of the Fe sputtering yield at this ion dose is due to the onset of Ag segregation, taking place during the ion-sculpting process itself, favored by both the local heating and the intermixing effect due to the ion impacts.[22] The Ag segregation intuitively leads to a decrease of the Fe-selective sputtering yield measured by I_{sat}, via mechanisms analogous to the ones taking place at $\Phi<2$ MLE. This interpretation is supported by the observation of AES spectra that clearly show an increase of the intensity of the Ag line starting from around 10 MLE. The exact amount of Ag segregated at the film surface or mixed in the interior of the film due to the local ion-induced heating is an experimental quantity which is extremely difficult to quantify. In this respect, the film morphology at an ion dose above 10 MLE eludes a precise characterization with our available experimental techniques.

B. Magnetic anisotropy

The total uniaxial magnetic anisotropy K_u of the rippled Fe/Ag(001) system is the sum of different contributions.[6] The magnetocrystalline term K_u^{mc} is due to the imbalance in

the densities of steps parallel and perpendicular to the ripple ridges, induced by the ripple morphology itself. The magnetostatic contribution (shape anisotropy) K_u^{ms} originates from the difference between the energy stored in the demagnetizing field in the case of magnetization parallel and perpendicular to the ripple direction. Besides the above contributions, a magnetoelastic term K_u^{me} can be induced by mesoscopic relaxation phenomena brought about by the ripple morphology.[32]

The monotonous increase of the total anisotropy K_u for an ion dose up to 10 MLE results from the gradual buildup of the density of atomic steps along the [100] direction, along with gradually increasing magnetostatic and magnetoelastic contributions. The remarkably different evolution of K_u observed above 10 MLE on the other hand, can be ascribed to the ion-induced segregation and interdiffusion of Ag atoms, affecting the film and surface electronic properties. In fact, in that ion-dose range the proximity of the surface of the Fe film with the buried Fe-Ag interface may lead to sputter-induced intermixing as observed in x-ray photoelectron spectroscopy[20] (XPS) and low-energy ion scattering[22] (LEIS) depth-profile experiments. However, the previously mentioned uncertainty in the determination of the film morphology in this ion-dose range does not allow any discussion beyond this qualitative level. In the following, we will therefore focus our attention more deeply on the low-dose regime.

We begin our analysis by considering contributions to the uniaxial anisotropy other than K_u^{mc}, namely, magnetostatic and magnetoelastic effects. For an ideal ripple structure, the magnetostatic anisotropy can be precisely quantified with the aid of micromagnetic calculations. In real systems, however, the surface uncorrelated roughness and the finite in-plane aspect ratio of surface ripples concur to decrease the experimental shape anisotropy with respect to the ideal case.[6,33] The actual amount by which K_u^{ms} is decreased is, however, by no means easy to determine, thus yielding great inaccuracies in the computational determination of the shape anisotropy. Evaluation of eventual magnetoelastic contributions, due to the mesoscopic relaxation mechanisms, is beyond the state-of-the-art experimental and computational capabilities. In order to yield a reasonable estimate of K_u^{ms} and K_u^{me}, given the difficulties in computing the magnitude of such contributions to uniaxial anisotropy, we chose to experimentally set their upper limit by means of adsorption experiments. In detail, we monitored the adsorbate dependence of the total anisotropy K_u as a function of the exposure to gaseous molecular oxygen. For very low exposure, for which only the surface is affected by the adsorbate, we do not expect the nanoscale morphology to be modified, thus leaving the shape anisotropy unchanged. Similarly, mesoscopic strain is not affected by low adsorbate coverage, thus leaving K_u^{me} unchanged. All the variations of the uniaxial anisotropy in the low exposure regime must then be due to a variation of the magnetocrystalline term, thus providing a way to separate the contribution of K_u^{mc} from K_u^{ms} and K_u^{me}. We have monitored the O_2-exposure dependence of the uniaxial anisotropy of two different 24-ML-thick Fe/Ag(001) films, irradiated with ion doses of 4 and 5.5 MLE, respectively, which is in the ion-dose window for which well-defined ripple morphology is deduced from SPA-LEED data. Exposure was performed at a temperature of 350 K. For both samples, the adsorbate-coverage dependence of K_u exhibited a minimum in correspondence of an exposure of about 1 L of O_2 (1 L $=10^{-6}$ torr s), whose value amounted in both cases to 15% of the clean-surface value of K_u (full diamonds, bottom panel of Fig. 3). If we assume that K_u^{mc} does not change sign upon oxygen adsorption, the minimum of K_u sets the *upper limit* of the combined magnetostatic and magnetoelastic anisotropy for ion doses of 4 and 5.5 MLE, respectively. In the case where oxygen quenches K_u^{mc}, the total residual anisotropy has magnetostatic and/or magnetoelastic origin, whereas in the case where oxygen merely reduces K_u^{mc}, the magnetostatic and/or magnetoelastic contribution will just be a fraction of the residual anisotropy. Whatever the case, the minimum value of the total anisotropy K_u can be safely treated as an upper limit of the combined contribution $K_u^{ms}+K_u^{me}$. Given the small relative weight of $K_u^{ms}+K_u^{me}$ with respect to the total anisotropy K_u, we will treat the residual magnetostatic and/or magnetoelastic anisotropy as an effective experimental uncertainty in the evaluation of K_u^{mc}.

We then focus our attention on extracting the numerical value of the step-induced magnetocrystalline uniaxial anisotropy per unit step length from our experimental data. Assuming a triangular envelope for the ripple profile,[6] the step-induced magnetocrystalline anisotropy can be written as

$$K_u^{mc} = \kappa_u^{mc} \frac{\tan \alpha(\Phi)}{t(\Phi) d^2}, \tag{2}$$

where κ_u^{mc} is the step-induced uniaxial magnetocrystalline anisotropy per unit step length, $\alpha(\Phi)$ is the slope of the ripple facets at ion dose Φ, $t(\Phi)$ is the ion-dose-dependent average film thickness (expressed in ML), and d is the monatomic step height for Fe.

Since we are interested in measuring the magnetocrystalline anisotropy κ_u^{mc} of *clean* and possibly defect-free Fe monatomic steps, we limit ourselves to the quantitative analysis of experimental data in the 2–6 MLE ion-dose interval [indicated as region (a) in the bottom panel of Fig. 3], for which these requirements are fulfilled. In fact, for an ion dose up to approximately 2 MLE, the application of Eq. (2) is not justified due to the incomplete development of the triangular ripple envelope assumed there. In addition, the residual presence of Ag on the surface prevents the fulfilling of the cleanliness condition stated above. For an ion dose in excess of approximately 6 MLE, both the proximity to the substrate and the accumulation of uncorrelated roughness suggest that the amount of defects in the films might lead to an incorrect estimation of the magnetic anisotropy. In the 2–6 MLE interval, the ion-dose-dependent facet slope is obtained by linear regression of the data reported in Fig. 1(d) (straight solid line), whereas the average thickness $t(\Phi)$ is deduced from the linear fit of I_{sat} displayed in Fig. 3. As suggested by the adsorption data, we assume the *relative* contribution of the magnetostatic and/or magnetoelastic anisotropy to be identical for all the data points in the range, accounting for at most 15% of the total anisotropy. The numerical values of the ion dose, the magnetocrystalline anisotropy, the thickness, and the slope employed to calculate κ_u^{mc} are reported in Table I.

TABLE I. Numerical values of the magnetocrystalline anisotropy K_u^{mc}, the average film thickness, the ripple slope, and the step-induced uniaxial anisotropy per unit length in the 2.65–5.5 MLE ion-dose interval. The values of K_u^{mc} reported here consider a relative shape anisotropy contribution to the total uniaxial anisotropy of 15%.

Φ (MLE)	K_u^{mc} (10^4 erg/cm^3)	t (ML)	α (deg)	κ_u^{mc} (10^{-10} erg/cm)
2.65	2.16	24.0	12.2	4.9
3.35	2.44	22.2	12.6	4.9
4.05	3.19	20.8	13.0	5.8
4.75	4.28	19.4	13.4	7.1
5.50	5.07	18.0	13.9	7.5

From these values, we obtain a lower limit of $\kappa_u^{mc}=(6\pm1)\times10^{-10}$ erg/cm (assuming a 15% contribution of magnetostatic and/or magnetoelastic anisotropy) and an upper limit of $\kappa_u^{mc}=(7\pm1)\times10^{-10}$ erg/cm (neglecting magnetostatic and/or magnetoelastic anisotropy). Treating the indetermination in the relative weight of the shape anisotropy as an effective experimental uncertainty, we obtain a value of $\kappa_u^{mc}=(6.5\pm1.5)\times10^{-10}$ erg/cm. We notice that the value of κ_u^{mc} that we extract from our experimental data shows the systematic tendency to increase for increasing dose. We propose that this effect is due to the gradual increase in the amount of atoms located in low-coordinated sites such as step adatoms, which, due to their different local environments, contribute differently to the magnetic anisotropy with respect to straight steps. This observation fully justifies our choice to set an upper limit to the ion dose at 5.5 MLE for the quantitative analysis of the step-induced anisotropy. We stress that the value of κ_u^{mc} that we obtain corresponds to the in-plane projection of the total step-induced magnetic anisotropy energy. The measurement of the out-of-plane component of the step-induced anisotropy was not attempted in this work.

The comparison of our findings with the experimental values of the step-induced anisotropy in Fe/Ag(001) films reported in the literature has to be performed with particular care. In fact, whereas the largest part of the studies of step-induced anisotropy has been performed on vicinal systems, our study follows a different approach. In detail, it was, in fact, recently shown that the uniaxial magnetic anisotropy of vicinal Fe/Ag(11n) films does not originate from surface steps, but rather from bulklike lattice distortions,[14] while measurements from ion-sculpted films allow the step-induced anisotropy to be correctly isolated.[10] Accordingly, the experimental value $\kappa_u^{mc}=5.73\times10^{-8}$ erg/cm, measured for the Fe/Ag(11n) system,[13] should not be considered as a selective measurement of the magnetic anisotropy due to surface steps, as later demonstrated.[10,14] The overestimation of κ_u^{mc} in Ref. 13 arose from incorrectly ascribing to surface steps the uniaxial anisotropy generated via magnetoelastic effects all over the thickness of the magnetic film. Within this framework, the difference of 2 orders of magnitude between the step-induced anisotropy measured in the present experiment and in Ref. 13 should not be regarded as a discrepancy. Coming to the Fe/MgO(001) system, which has close analogies to Fe/Ag(001), we also find experimental studies of the uniaxial anisotropy of in-plane patterned films that, however, do not report any value of the magnetocrystalline step-induced anisotropy.[34,35] In this respect, we believe that the present work highlights the role of magnetocrystalline anisotropy of surface origin in the Fe/Ag(001) system, yielding an estimation of its magnitude free of bulklike undesired contributions.

We explicitly chose *not* to provide the value of the uniaxial magnetocrystalline anisotropy in terms of the magnetic anisotropy energy per atom, in order to take into account the possibility of nonlocal contributions to the step-induced uniaxial anisotropy. Indeed, although calculations performed within the framework of Néel's next-neighbor model showed that only one type of atom at the step contributes to the uniaxial anisotropy,[36] the local approximation employed there is extremely unlikely to hold for itinerant 3d electrons. In this respect, we believe that the present work will stimulate further research in this direction.

V. CONCLUSION

In conclusion, we have provided a quantitative estimate of the magnitude of the step-induced in-plane magnetic uniaxial anisotropy in ultrathin Fe/Ag(001) films nanostructured by the ion-sculpting technique. We find a value for the magnetocrystalline anisotropy per unit step length $\kappa_u^{mc}=(6.5\pm1.5)\times10^{-10}$ erg/cm. The large difference observed with respect to the value deduced by experimental studies performed on vicinal systems[13] is ascribed to the presence, in the latter systems, of spurious contributions to the uniaxial anisotropy.[14] Within this framework, our finding represents a more reliable estimate of the step-induced uniaxial magnetocrystalline anisotropy and, as such, is a valuable benchmark for testing theoretical models of magnetic anisotropy in low-dimensional Fe-based systems and nanostructures.

ACKNOWLEDGMENTS

Financial support from the MIUR programs FIRB No. RBNE017XSW, FIRB No. RBNE01YLKN, and PRIN 2004029329 is acknowledged. F.B.d.M. acknowledges financial support from MAE under the Italy-Slovenia bilateral project.

*Electronic address: moroni@fisica.unige.it

[1] J. G. Gay and R. Richter, Phys. Rev. Lett. **56**, 2728 (1986).
[2] B. Heinrich, K. B. Urquhart, A. S. Arrott, J. F. Cochran, K. Myrtle, and S. T. Purcell, Phys. Rev. Lett. **59**, 1756 (1987).
[3] G. M. Pastor, J. Dorantes-Dávila, S. Pick, and H. Dreyssé, Phys. Rev. Lett. **75**, 326 (1995).
[4] B. Nonas, I. Cabria, R. Zeller, P. H. Dederichs, T. Huhne, and H. Ebert, Phys. Rev. Lett. **86**, 2146 (2001).
[5] P. Gambardella, S. S. Dhesi, S. Gardonio, C. Grazioli, P. Ohresser, and C. Carbone, Phys. Rev. Lett. **88**, 047202 (2002).
[6] R. Moroni, D. Sekiba, F. Buatier de Mongeot, G. Gonella, C. Boragno, L. Mattera, and U. Valbusa, Phys. Rev. Lett. **91**, 167207 (2003).
[7] S. Rusponi, T. Cren, N. Weiss, M. Epple, P. Buluschek, L. Claude, and H. Brune, Nat. Mater. **2**, 546 (2003).
[8] P. Gambardella, S. Rusponi, M. Veronese, S. S. Dhesi, C. Grazioli, A. Dallmeyer, I. Cabria, R. Zeller, P. H. Dederichs, K. Kern, C. Carbone, and H. Brune, Science **300**, 1130 (2003).
[9] P. Gambardella, A. Dallmeyer, K. Maiti, M. C. Malagoli, S. Rusponi, P. Ohresser, W. Eberhardt, C. Carbone, and K. Kern, Phys. Rev. Lett. **93**, 077203 (2004).
[10] F. Bisio, R. Moroni, F. Buatier de Mongeot, M. Canepa, and L. Mattera, Phys. Rev. Lett. **96**, 057204 (2006).
[11] A. Berger, U. Linke, and H. P. Oepen, Phys. Rev. Lett. **68**, 839 (1992).
[12] W. Weber, C. H. Back, A. Bischof, C. Würsch, and R. Allenspach, Phys. Rev. Lett. **76**, 1940 (1996).
[13] R. K. Kawakami, E. J. Escorcia-Aparicio, and Z. Q. Qiu, Phys. Rev. Lett. **77**, 2570 (1996).
[14] Y. Z. Wu, C. Won, and Z. Q. Qiu, Phys. Rev. B **65**, 184419 (2002).
[15] M. Rickart, T. Mewes, S. O. Demokritov, B. Hillebrands, and M. Scheib, Phys. Rev. B **70**, 060408(R) (2004).
[16] S. Rusponi, G. Costantini, F. Buatier de Mongeot, C. Boragno, and U. Valbusa, Appl. Phys. Lett. **75**, 3318 (1999).
[17] U. Valbusa, C. Boragno, and F. Buatier de Mongeot, J. Phys.: Condens. Matter **14**, 8153 (2002).
[18] M. Canepa, M. Salvietti, A. Campora, and L. Mattera, J. Electron Spectrosc. Relat. Phenom. **76**, 471 (1995).
[19] M. Canepa, S. Terreni, P. Cantini, A. Campora, and L. Mattera, Phys. Rev. B **56**, 4233 (1997).
[20] D. E. Bürgler, C. M. Schmidt, D. M. Schaller, F. Meisinger, R. Hofer, and H. J. Güntherodt, Phys. Rev. B **56**, 4149 (1997).
[21] D. M. Schaller, D. E. Bürgler, C. M. Schmidt, F. Meisinger, and H. J. Güntherodt, Phys. Rev. B **59**, 14516 (1999).
[22] M. Canepa, P. Cantini, O. Ricciardi, S. Terreni, and L. Mattera, Surf. Sci. **429**, 34 (1999).
[23] S. van Dijken, G. Di Santo, and B. Poelsema, Phys. Rev. B **63**, 104431 (2001).
[24] Z. Q. Qiu, J. Pearson, and S. D. Bader, Phys. Rev. Lett. **70**, 1006 (1993).
[25] F. Bisio, S. Terreni, M. Canepa, and L. Mattera, Phys. Rev. B **72**, 174413 (2005).
[26] F. Buatier de Mongeot, G. Costantini, C. Boragno, and U. Valbusa, Phys. Rev. Lett. **84**, 2445 (2000).
[27] F. Bisio, R. Moroni, F. Buatier de Mongeot, M. Canepa, and L. Mattera, Appl. Phys. Lett. **89**, 052507 (2006).
[28] W. Weber, R. Allenspach, and A. Bischof, Appl. Phys. Lett. **70**, 520 (1997).
[29] J. Zak, E. R. Moog, C. Liu, and S. D. Bader, J. Magn. Magn. Mater. **89**, 107 (1990).
[30] M. A. Makeev and A. L. Barabási, Nucl. Instrum. Methods Phys. Res. B **222**, 335 (2004).
[31] H. Hansen, C. Polop, T. Michely, A. Friedrich, and H. M. Urbassek, Phys. Rev. Lett. **92**, 246106 (2004).
[32] O. V. Lysenko, V. S. Stepanyuk, W. Hergert, and J. Kirschner, Phys. Rev. Lett. **89**, 126102 (2002).
[33] Y. P. Zhao, G. Palasantzas, G. C. Wang, and J. T. M. De Hosson, Phys. Rev. B **60**, 1216 (1999).
[34] H. Jaffrès, P. Le Fèvre, H. Magnan, A. Midoir, D. Chandesris, L. Ressier, A. Schuhl, F. Nguyen Van Dau, M. Goiran, J. P. Peyrade, and A. R. Fert, Phys. Rev. B **61**, 14628 (2000).
[35] J. H. Wolfe, R. K. Kawakami, W. L. Ling, Z. Q. Qiu, R. Arias, and D. L. Mills, J. Magn. Magn. Mater. **232**, 36 (2001).
[36] D. S. Chuang, C. A. Ballentine, and R. C. O'Handley, Phys. Rev. B **49**, 15084 (1994).